Korean J. Chem. Eng., 33(3), 1104-1114 (2016)
DOI: 10.1007/s11814-015-0202-z

pISSN: 0256-1115
eISSN: 1975-7220

Rheology, mechanical properties and crystallization behavior of glycidyl methacrylate grafted poly(ethylene octene) toughened poly(lactic acid) blends

Yan Zhao*,, Ye Zhang*,**, Zonglin Li**, Hongwei Pan**, Qinglin Dong**, Lijing Han**, Huiliang Zhang**,†, and Lisong Dong****

*Synthetic Resins and Special Fiber Engineering Research Center, Ministry of Education, Changchun University of Technology, Changchun 130012, China
**Key Laboratory of Polymer Ecomaterials, Chinese Academy of Sciences, Changchun Institute of Applied Chemistry, Changchun 130022, China
(*Received 27 June 2015 • accepted 22 September 2015*)

Abstract−Poly(lactic acid) (PLA)/poly(ethylene octene) grafted with glycidyl methacrylate (POE-g-GMA denoted as GPOE) blends were prepared via simple melt compounding method at GPOE loadings from 5 to 20 wt%. GPOE can significantly affect the physical properties of PLA. Compared to neat PLA, the elongation at break and impact strength of the blends were significantly improved. Scanning electron micrograph analysis revealed large numbers of cavities in the fracture surface of the blends, and the size of the cavities increased along with the increase of GPOE content in the PLA/GPOE blends. Furthermore, the overall crystallization rates were faster in the PLA/GPOE blends than that in neat PLA. However, the crystallization mechanism and crystal structure of these blends remained unchanged despite the presence of GPOE. The addition of GPOE decreased the degree of crystallinity of PLA. The toughened PLA could be of great use and importance for wider practical applications.

Keywords: PLA, GPOE, Blends, Mechanical Properties, Crystallization

INTRODUCTION

Poly(lactic acid) (PLA) is a thermoplastic aliphatic polyester which can be produced from annually renewable resources. It has a number of excellent properties including biodegradability, biocompatibility, good mechanical properties and processability. PLA has been widely used in biomedical materials and general plastics [1-4]. Nevertheless, the brittleness of PLA has limited its widespread applications. The toughening of PLA has been studied for a long time, and many different approaches have been used to improve its toughness [5-14]. For example, PLA is blended with other more flexible and biodegradable polymers such as PCL, PBS, poly(3-hydroxybutyrate) (PHB) and poly(butylene adipate-co-terephthalate) (PBAT) [15-18]. However, these materials prepared by simple blending still suffer from poor impact resistance due to the phase separation and poor interfacial adhesion between the two immiscible components.

Poly(ethylene octene) (POE) is a kind of flexible polymer which can be obtained through copolymerization of octene and ethylene. Compared with conventional polyolefin elastomers, such as ethylene-propylene-diene (EPDM) rubber, ethylenepropylene rubber (EPR) and polystyrene-b-poly(ethylene-ran-butylene)-b-polystyrene (SEBS), POE exhibits the advantage of thermoplastic processability [19,20]. Glycidyl methacrylate (GMA) grafted polymers are often used as reactive compatibilizer in polyester blends [21-24]. It is usually believed that epoxy groups can react with carboxyl or hydroxyl groups of polyester. The end hydroxyl and/or carboxyl groups of PLA can react with epoxy groups via nucleophilic substitution under appropriate conditions. Therefore, it is expected that GMA grafted poly(ethylene octene) (GPOE) will have a significant toughening effect on PLA.

In this study, PLA was blended with GPOE. The miscibility, rheological behavior, mechanical properties, and crystallization behavior of the PLA/GPOE blends were investigated. This work aims at assessing the miscibility, phase morphology, toughening mechanisms and the crystallization behavior of the PLA/GPOE blends.

EXPERIMENTAL

1. Materials

PLA (4032D) was obtained from Natureworks™ in pellet form with a weight-average molecular weight (M_w) of 207,000, polydispersity of 1.73. The GMA grafted POE (GPOE, grafted ratio is 2.5 wt%, chemical structure as shown in Scheme 1) contained 25% by weight of octene was kindly supplied by Ketong Plastic Co., Ltd. (Shenyang, China).

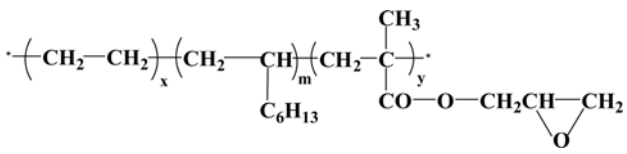

Scheme 1. Structure of GPOE.

†To whom correspondence should be addressed.
E-mail: hlzhang@ciac.jl.cn

2. Blends Preparation

PLA was dried at 80 °C for 8 h and GPOE was dried at 50 °C for 5 h in a vacuum oven, respectively. PLA/GPOE blends were prepared by melt compounding with a Haake Rheomix 600 (Karlsruhe, Germany) at a rotating speed of 60 rpm at 185 °C for 5 min. The mixing compositions of the PLA/GPOE blends were 95/5, 90/10, 85/15, 80/20 w/w. Also, the neat PLA was subjected to the same mixing treatment to create the same thermal history as that of the blends. After mixing, all of the compounds were cut into small pieces. Then, all of samples were compression-molded into sheets with thicknesses of 1.0 mm and width of 4.0 mm at 185 °C for various tests. The hydraulic press was set at 120 kg/cm^2.

3. Fourier Transform Infrared Spectroscopy

Fourier transform infrared ray (FT-IR) spectroscopy (Nicolet 6700, USA) was used to investigate the intermolecular interaction between PLA and GPOE. Prior to FTIR measurements, the samples for the blends were extracted in hot xylene for 20 h and in chloroform for another 20 h. Spectra were obtained at 4 cm^{-1} resolution and averages were obtained from 64 scans in the standard wave number range from 500 to 4,000 cm^{-1}. All samples were dried under vacuum at 50 °C for 8 h before testing.

4. Rheological Properties

Rheological measurements of the blends were on a Physica MCR 2000 rheometer (AR 2000ex). Frequency sweep for the neat PLA and PLA/GPOE samples was under nitrogen using 25-mm plate-plate geometry. The gap distance between the parallel plates was 0.9 mm for all tests. The sheet samples were about 1.0 mm in thickness. A strain sweep test was initially conducted to determine the linear viscoelastic region of the materials. The angular frequency range used during testing was 0.1-100 rad/s. The temperature was plotted at 185 °C.

5. Mechanical Properties Test

Uniaxial tensile tests were carried out on dumbbell shaped specimens (W×H×L=4×1×20 mm^3), which were punched out from the compression-molded sheets. The measurements were performed using a tensile-testing machine (Instron-1121, Canton, MA) according to ASTM D638-2008 at a crosshead speed of 20 mm/min. All tests were carried out at room temperature and 50% relative humidity. At least five specimens were tested for each sample to get an average value.

Notched Izod impact tests were performed at 23±2 °C according to ASTM D256-2010 on an impact testing machine (CEAST, Chengde, China). The samples with dimensions 63.5×12.7×4.0 mm^3 were obtained from compression-molded specimens. The notch was milled in having a depth of 2.54 mm, an angle of 45°, and a notch radius of 0.25 mm.

6. Morphology of Blends

The morphology of the neat PLA and PLA/GPOE blends was characterized with a scanning electron microscope (model Japan JXA-840 ESEMFE). A layer of gold was sputter-coated uniformly over all the fractured surfaces before SEM observations.

7. Thermal Properties

Crystallization behavior of the composites was studied by differential scanning calorimetry (DSC) (TA Instruments DSC Q20 USA) with the specimens sliced from blown blend samples. The heating and cooling rates were 10 °C/min with nitrogen purge, and the sample weights were between 5 and 8 mg. The samples were heated first from −50 up to 190 °C at 10 °C/min and held at 190 °C for 3 min to eliminate their previous thermal history, then cooled at the same rate and finally heated again. As GPOE is amorphous, only the contribution of the PLA was considered. The degree of crystallinity of the samples was evaluated from the heat evolved during crystallization by the following relationship:

$$x_c = \frac{\Delta H_f}{w_{PLA} \times \Delta H_f^0} \times 100\% \quad (1)$$

where x_c is the degree of crystallinity of the samples, ΔH_f is the heat of fusion of the PLA in the blend, ΔH_f^0 is the heat of fusion for 100% crystalline PLA (93 J/g) [25] and w_{PLA} is the weight fraction of PLA in the blend.

The isothermal melt crystallization of PLA/GPOE blends has been studied. The samples (about 7.0 mg) were heated first from 0 to 190 °C at 50 °C/min, and held at 190 °C for 3 min, then cooled to the desired crystallization temperature at 45 °C/min and held until the isothermal crystallization was complete. The crystallization temperatures chose in this work were 100, 105 and 110 °C, respectively.

8. Crystalline Morphology

The crystallite morphology of PLA/GPOE samples was observed with a Leica DMLP polarized microscope (POM) equipped with a Linkam TM600 hot stage and a computer-controlled charged-coupled-device camera. A small amount of sample with a thickness of approximately 0.05 mm was sandwiched between two microscope cover glasses and then placed on the hot stage. The samples were heated from room temperature to 190 °C at a rate of 30 °C/min, held there for 5 min to eliminate previous thermal history, and then quenched to 110 °C at a rate of 30 °C/min for isothermal crystallization and held for 60 min. The morphology changes were recorded during the crystallization process.

9. X-ray Analysis

Wide angle X-ray diffraction (WAXD) experiments were performed on a D8 advance X-ray diffractometer (Bruker, Germany) at room temperature in the range of 5-40° at a scanning rate of 4°/min. The Cu Kα radiation (λ=0.15418 nm) source was operated at 40 kV and 200 mA.

Small-angle X-ray scattering (SAXS) experiments of undeformed specimens were performed at RT using a NanoSTAR-U (Bruker AXS Inc.) with Cu Kα radiation (wavelength, λ=0.154 nm). The generator was operated at 40 kV and 650 μA. Two-dimensional SAXS patterns were obtained with a HI-STAR detector. The sample-to-detector distance was L_{SD}=1074 mm. The effective scattering vector q (q=$(4\pi/\lambda)\sin\theta$, where 2θ is the scattering angle) at this distance ranged from 0.044 to 2.0 nm^{-1}. The X-ray exposure time was 60 min. Before testing, the samples were prepared by using a hot press at 190 °C and a hold time of 5 min, followed by annealing at 110 °C for 1 h.

RESULTS AND DISCUSSION

1. Reaction Mechanism

In Fig. 1, the FTIR spectra of neat PLA, neat GPOE, and the 80/20 PLA/GPOE blend are illustrated to elucidate the structural changes

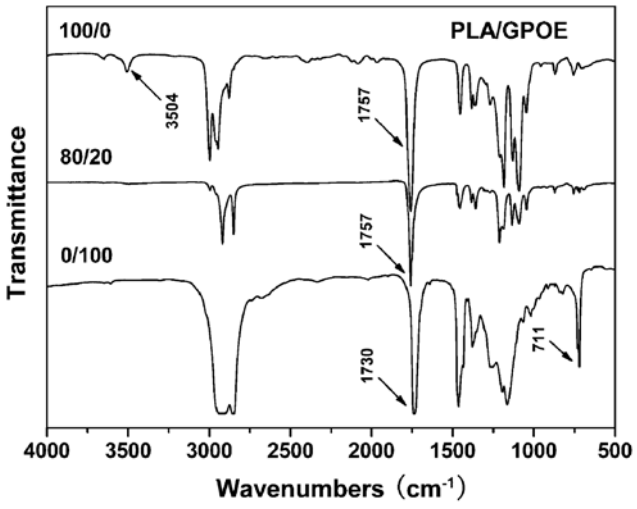

Fig. 1. FTIR spectra of neat PLA, neat GPOE and PLA/GPOE blend.

induced by the reaction between carboxylic acid and epoxy during the melt-processing. Prior to FTIR test, the 80/20 PLA/GPOE blend was extracted in xylene and chloroform to remove the unreacted GPOE and PLA, respectively. For the 80/20 PLA/GPOE blend, it shows that the absorption at 3,504 cm^{-1} belongs to the end carboxylic group of PLA disappeared, which confirmed the chemical reaction between the end carboxylic acid group of PLA and the epoxide group of GPOE. The strong absorption at 1,757 cm^{-1} was attributed to the stretch vibration of ester carbonyl group of the PLA backbone, while the vibration of ester carbonyl of GMA in GPOE was located at 1,730 cm^{-1}. With increasing GPOE content in the blends, the intensity of absorption peak at 1,757 cm^{-1} increased and the absorption peak of ester carbonyl for GPOE disappeared. Compared with neat GPOE, the intensity of the epoxy characteristic peak at 711 cm^{-1} decreased. It suggested that most of the GPOE was reacted with PLA [26].

2. Rheological Properties

Rheological behavior played an important role in polymer processing. As it is known, polymer material processing especially requires a relative high melt strength. Dynamic rheological experiments were carried out for the PLA/GPOE blends over the whole composition range. As shown in Fig. 2(a), the dynamic storage modulus G′ of PLA/GPOE blends increased with increasing angular frequency and also increased with increasing GPOE content in the blends. At low frequencies, compared with neat PLA the G′ of the 80/20 PLA/GPOE blend increased by about an order of magnitude. The higher absolute values of dynamic modulus indicated the formation of interaction and entangled structures of molecular chains between PLA and polyolefin elastomer [27-30].

Fig. 2(b) shows the relationship between complex viscosity η^* and angular frequency of the PLA/GPOE blends at 185 °C. With increasing the angular frequency, all composites showed shear-thinning behavior, which was mainly ascribed to the disentanglement of molecular chain between PLA and GPOE at high shearing rate. At low frequencies, the addition of GPOE resulted in a gradual increase in the viscosity of the blends. The η^* of the PLA/GPOE blends was much higher than that of the neat PLA due to the interaction between PLA and GPOE. The entanglements of molecular chains took place between PLA and polyolefin elastomer. The melt viscosity of the PLA/GPOE blends increased with increasing GPOE content because more GPOE obstacles existed and more PLA chains had been anchored at low shear rates. This significant enhancement in the melt viscosity of PLA/GPOE blends led to an enhancement in melt strength, which was favorable for the processing of blown

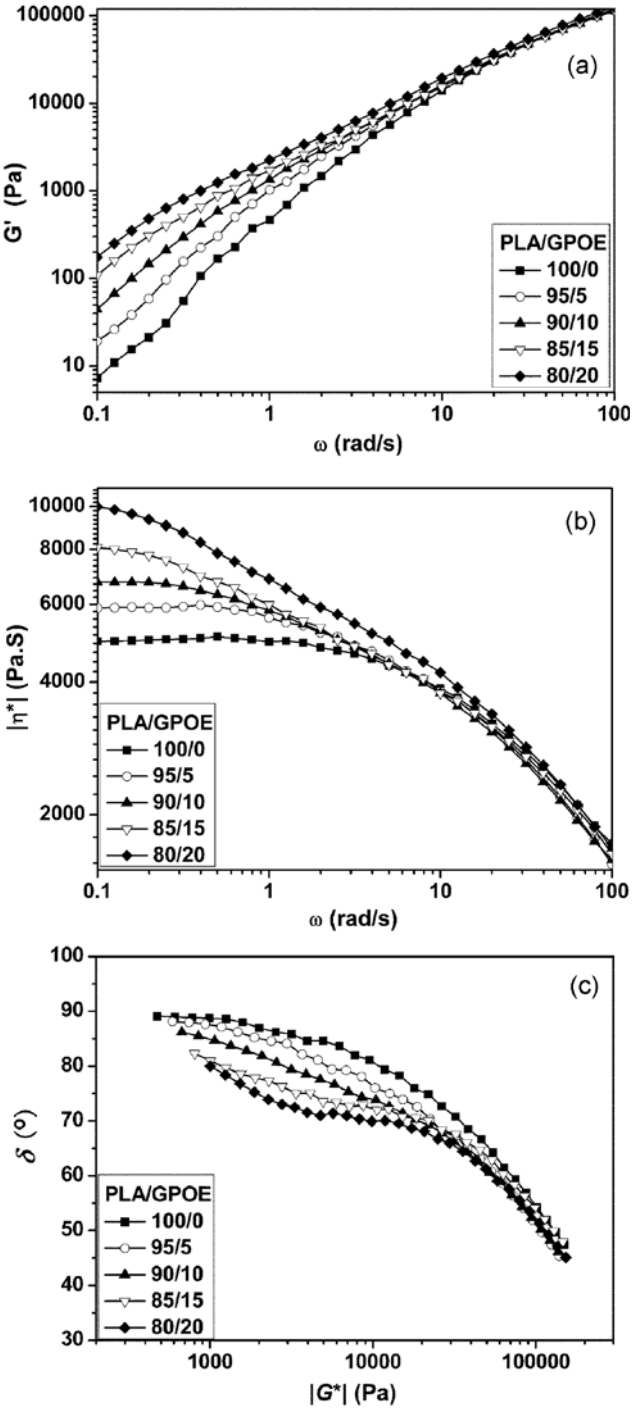

Fig. 2. Frequency dependence of (a) storage modulus (G′), (b) complex viscosity (η^*), and (c) the phase angle (δ) for neat PLA and PLA/GPOE blends.

Table 1. Mechanical properties of PLA/GPOE blends

PLA/GPOE (w/w)	Young's modulus (MPa)	Tensile strength (MPa)	Elongation at break (%)	Notched impact strength (kJ/m^2)
100/0	1377±164	53.5±1.1	4.5±0.8	3.5±0.7
95/5	1211±124	43.9±1.4	17.9±1.3	17.1±2.2
90/10	1129±143	40.1±1.8	90.6±17.2	41.8±3.4
85/15	844±172	33.8±1.9	157.2±13.4	60.3±2.5
80/20	556±117	22.1±1.0	264.3±16.1	69.9±1.3

blends. At high frequencies, the η^* of the PLA/GPOE blends was decreased due to the disentanglement of molecular chains between PLA and GPOE.

In Fig. 2(c), the phase angle, δ, is plotted versus the absolute value of the complex modulus $|G^*|$ for the neat PLA and PLA/GPOE blends. This plot is known as van Gurp-Palmen plot, which can be used to detect the rheological percolation of the filled polymeric composites [31-33]. The low-frequency δ of the neat PLA was close to 90°, which is an indication of a flow behavior presented by the viscoelastic fluid. However, the low-frequency δ decreased to 80° with increasing GPOE content to 20 wt%, indicating an enhanced elastic behavior. Thus, the enhanced elastic behavior would be a benefit for blend blowing during the practical production process.

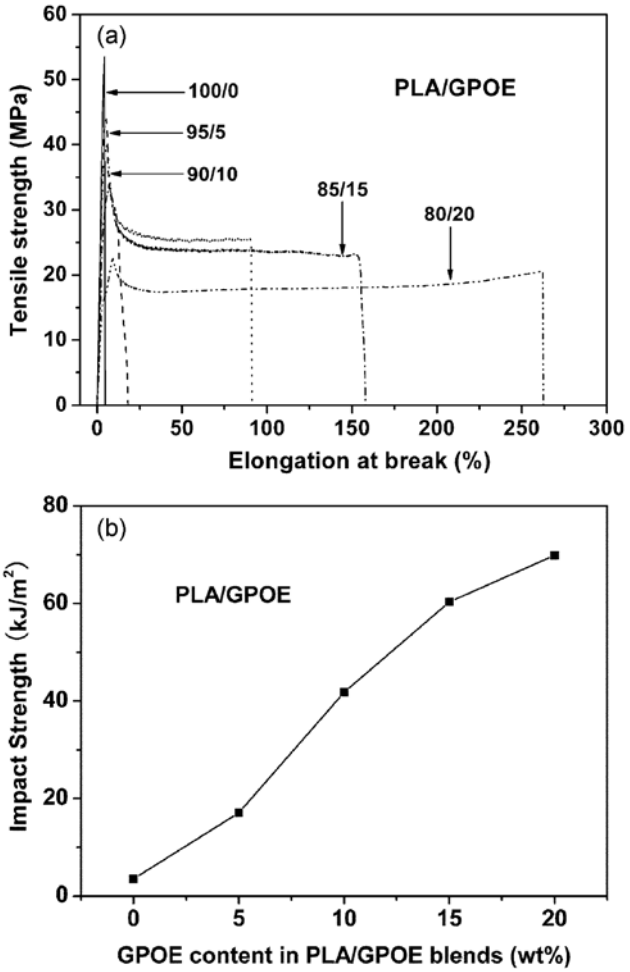

Fig. 3. Mechanical test: (a) Tensile behavior of neat PLA and PLA/GPOE blends, (b) notched impact strength of neat PLA and PLA/GPOE blends.

3. Mechanical Properties Test

The tensile properties and impact strength of neat PLA and PLA/GPOE blends are given in Table 1. The addition of GPOE changed the tensile behavior of the PLA significantly, as shown in Fig. 3(a). The tensile strength and the elongation at break of neat PLA were 53.5 MPa and 4.5%, respectively. The neat PLA showed brittle fracture upon tensile load. In contrast, all of the PLA/GPOE blends showed clear stress-strain curve yielding behavior. After yielding occurred, the strain developed continuously while the stress remained almost constant. The samples finally broke with a high elongation compared with that of neat PLA. It was very interesting to find that the 80/20 PLA/GPOE blend had a very high elongation at break of 264.3%, while the tensile strength remained as high as 22.1 MPa.

Measuring Young's modulus was the common method of determining the stiffness [34]. From Table 1, the neat PLA blend exhibited a modulus value of 1,377 MPa. The addition of GPOE decreased the modulus of PLA/GPOE blends. When the content of GPOE increased from 5% to 20%, the modulus decreased from 1,211 MPa to 556 MPa. This indicated that GPOE could improve the flexibility of PLA/GPOE blends.

Note that the impact strength of the blends was strengthened in Fig. 3(b). The neat PLA was so brittle it only had impact strength of 3.5 kJ/m^2. In contrast, the PLA/GPOE blends revealed a substantial increase in impact strength values as their GPOE content increased. For example, with increasing GPOE content from 5 to 20 wt%, the impact strength values of PLA/GPOE specimens were increased from 17.1 to 69.9 kJ/m^2. The brittle-ductile transition of the blends was obtained when the GPOE content varied from 5 to 10%.

These results suggested that the relatively poor impact strengths of the PLA could be significantly improved after melt blending with GPOE. Thus the physical entanglement increased by the incorporation of GPOE was conducive to enhancing the intermolecular force of the blends. For the PLA/GPOE blends, the great improvement of tensile strain at break and impact strengths might be ascribed to the intrinsic high flexibility of GPOE and the increased miscibility of two components due to the reaction between carboxyl of PLA and epoxy of GPOE. PLA was compatible with GPOE, which typically improved the impact strength by absorbing the energy of the impact through deformation of the elastomer. It could be used to improve the impact strength of the blends.

Surprisingly, the elastomer in the PLA/GPOE blends was found to yield a highly desired combination of high elongation at break, high impact strength and low Young's modulus required for most

market applications. For example, PLA could be used for manufacturing blown film. The PLA films for packaging applications were commonly made through a blown film process. In most applications, packaging films are required to possess high strength. The PLA/GPOE blends showed excellent flexibility and mechanical properties. GPOE will have a significant toughening effect on PLA films, which may be of great use and importance for the widely practical application of the PLA/GPOE blends.

4. Morphology of Blends

To further investigate the toughening mechanism of the PLA/GPOE blends, the morphology of different necking regions of the tensile specimen was cryofractured longitudinally to verify the interfacial adhesion effect on the micromechanical deformation processes. Neat PLA had almost the same smooth fracture surface in different regions without visible plastic deformation in the stress direction. However, the PLA/GPOE blends showed different behaviors under tensile testing. The different deformation stages of the 80/20 blend during stretching are presented in Fig. 4(a). The GPOE particles act as stress concentrators because they have an elastic property that differs from the PLA matrix. The consequent stress concentration leads to the development of a triaxial stress in the GPOE particles. The fractured morphology of the region that of the specimen where did not experience the tensile stress is shown in Fig. 4(b), many cavities can be seen on the fractured surface. Once the voids are formed, the hydrostatic stress state caused by stress concentration is released with the stress state in the ligaments of PLA between the voids being converted from a triaxial to more biaxial or uniaxial tensile stress state. With the continuous growth of voids, weak shear bands form in the matrix between the GPOE particles. At this stage, these cavities are enlarged along the stress direction, as shown in Fig. 4(c). With the continuous plastic growth of voids, PLA matrix between the GPOE particles deforms more easily and therefore shear yielding is achieved. The oriented cavities in the stress direction along with the deformation of the matrix are shown in Fig. 4(d). The plastic deformation, occurring via debonding process, is an important energy-dissipation process and leads to a toughened polymer blend. To conclude, the compatibility between the dispersed GPOE phase and PLA matrix in the blending process is necessary for toughness.

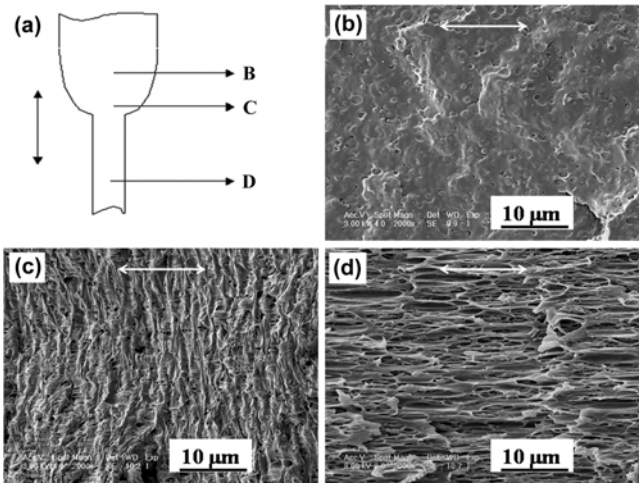

Fig. 4. (a) Schematic diagram of the measurement locations B, C, and D of the SEM micrographs of the PLA/GPOE blend (80/20) during the tensile testing; (b) morphology in region B; (c) morphology in region C; and (d) morphology in region D. The arrow indicates the stretching direction (10-μm scale bar).

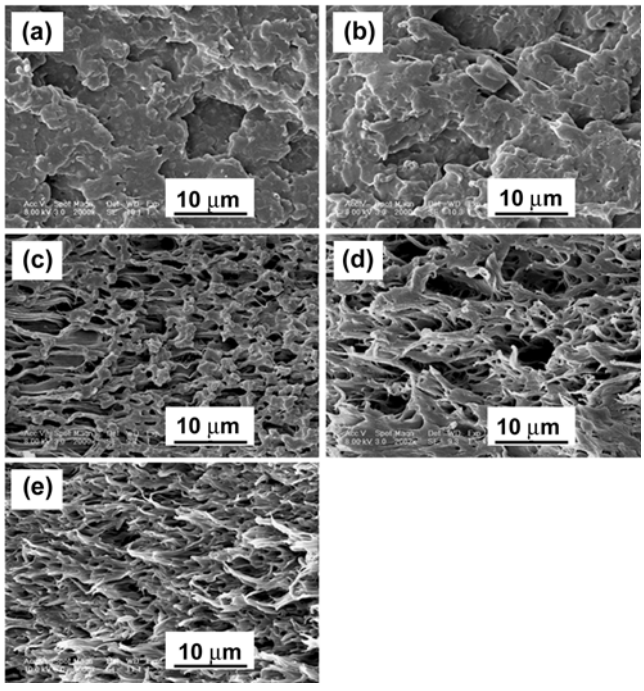

Fig. 5. SEM micrographs of the impact fracture surface of neat PLA and PLA/GPOE blends: (a) 100/0; (b) 95/5, (c) 90/10, (d) 85/15 and (e) 80/20.

SEM micrographs of the impact fracture surface of neat PLA and PLA/GPOE blends are given in Fig. 5. The fracture surface of neat PLA and 90/10 PLA/GPOE blend (Fig. 5(a)-(b)) shows a brittle fracture surface, indicating that the fractures are brittle during the impacting test. This is in good agreement with their lower elongation at break. When the GPOE content was 10%, as shown in Fig. 5(c), the surface began to become rough, more cavities could be seen obviously, and large area plastic deformation was observed, which suggested that the impact specimen broke yieldingly. Some cavitations and a clear matrix deformation can be clearly identified for the PLA/GPOE blends. These cavities are formed when the volumetric strain energy released by forming voids is greater than the surface energy needs to form a new surface. The energy needs to stretch the surrounding rubber to make space for the voids [35]. There are no clear gaps between the particles and the PLA matrix, suggesting some kind of interaction between PLA and GPOE. Especially, when the GPOE content reached 15 and 20%, the impact caused not only the cavities and matrix deformation but also some root-like whiskers. The 85/15 and 80/20 PLA/GPOE blends display significantly ductile fracture on which a rumpled surface can be seen (Fig. 5(d)-(e)). The rumples lie parallel to the notch of highly drawn material. The occurrence of rumples can be ascribed to the considerable impacting ahead of the crack tip before unstable fracture sets in. The extensive deformation ahead of the crack tip gives

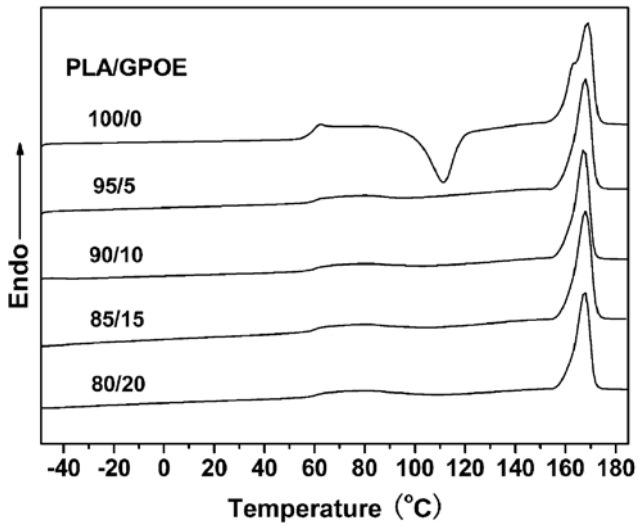

Fig. 6. DSC thermograms for PLA/GPOE blends with compositions from 100/0 to 80/20 in the second heating run.

Table 2. Crystallization properties of pure PLA and PLA/GPOE blends

PLA/GPOE (w/w)	Second heating run					
	T_g (°C)	T_{cc} (°C)	ΔH_{cc} (J/g)	T_m (°C)	ΔH_f (J/g)	X_c (%)
100/0	61.92	113.5	32.79	170.8	41.89	45.04
95/5	61.89	—	—	169.9	35.20	39.84
90/10	61.86	—	—	169.8	32.41	38.72
85/15	61.59	—	—	169.7	30.06	38.02
80/20	61.44	—	—	169.6	28.38	36.14

ΔH_f^0 of PLA is 93 J/g

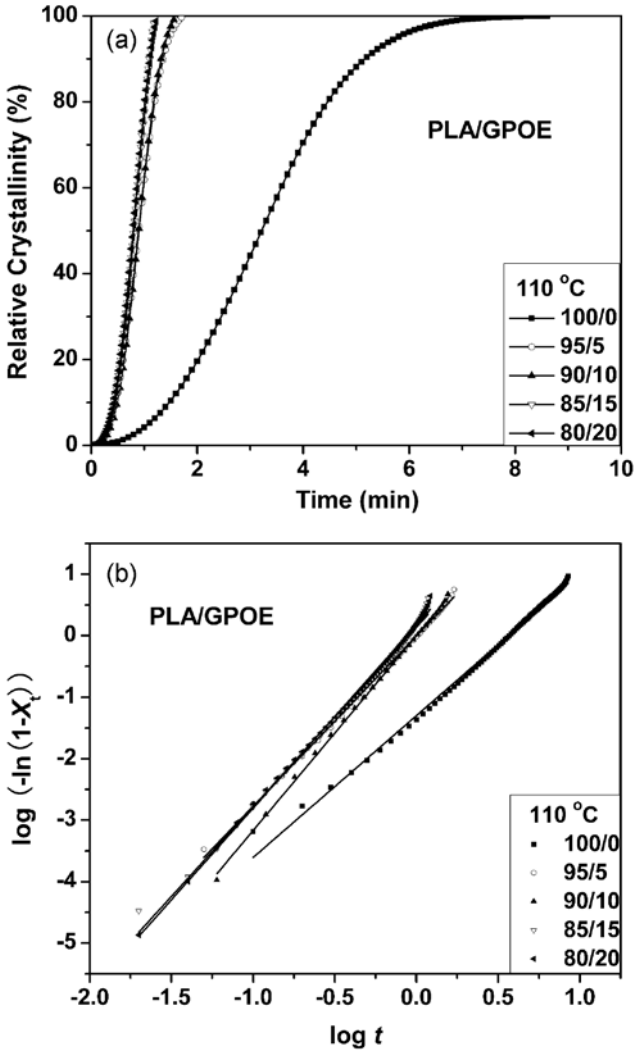

Fig. 7. (a) Variation of relative crystallinity with crystallization time for neat PLA and various blends at 110 °C and (b) the related Avrami plots.

rise to these structures. In particular, extensive plastic deformation in the PLA matrix can be clearly observed, which implies that shear yielding took place in the PLA matrix. This is a typical feature of a ductile fracture [27,36]. The SEM results of the impact fractures of the blends are in good agreement with the mechanical analysis.

5. Thermal Properties

The DSC heating thermograms shown in Fig. 6 exhibit two main transitions successively: a glass transition and a melting endotherm. The measured values of the phase transition parameters are summarized in Table 2.

Compared with neat PLA, the glass transition temperatures of the PLA/GPOE blends decreased slightly with increasing GPOE content in the blends. This indicated that the reaction between the two polymers had produced compatibilization effect and the PLA amorphous region was affected by GPOE. As shown in Scheme 2, after reactive compatibilization between PLA and GPOE, on one hand, with the addition of GPOE, the chains of entangled structures would decrease the space between polymer chains. Accord-

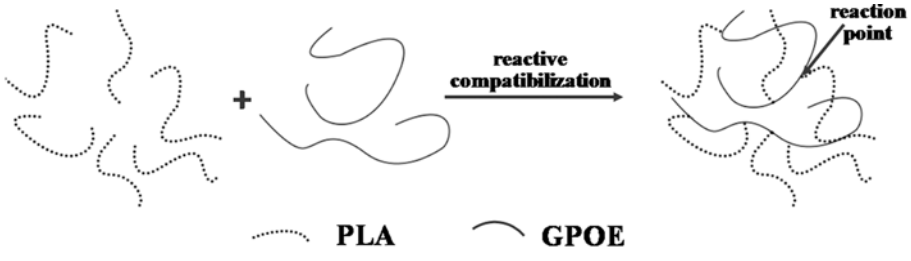

Scheme 2. Interaction mechanism diagram of PLA and GPOE.

ingly, the chain mobility of the polymer segments would be restricted during heating trace, so the glass transition temperature decreased. On the other hand, the chains of entangled structures resulted in more defective crystals; therefore, the T_m would shift to lower temperatures. In addition, the reaction point worked as a physical cross-linking point, entangled structures in amorphous area impeded the transportation of macromolecular chains between polymer chains, restricting the crystalline ability of PLA and forming more amorphous phase.

6. Isothermal Melt Crystallization

It is of great interest to investigate the addition of GPOE on the crystallization of PLA/GPOE blends. As introduced earlier, the overall isothermal crystallization kinetics of neat PLA and PLA/GPOE blends was studied by DSC from 100 to 110 °C. Fig. 7(a) shows the plots of relative crystallinity against crystallization time at 110 °C. The time-dependent relative degree of crystallinity X_t is calculated according to the following equation:

$$X_t = \frac{\int_0^t \frac{dH_c}{dt} dt}{\int_0^\infty \frac{dH_c}{dt} dt} \quad (2)$$

where dH_c/dt is the heat flow at time t.

In Fig. 7(a), all these curves have a similar sigmoid shape. The corresponding crystallization time for the PLA/GPOE blends was shorter than that of neat PLA, indicating a nucleation effect of GPOE as reported previously [25]. For example, it took the neat PLA sample almost 3.11 min to complete crystallization at 110 °C; however, for the PLA/GPOE5, PLA/GPOE10, PLA/GPOE15 and PLA/GPOE20 blends, the time required to finish crystallization was only around 0.88, 0.82, 0.79 and 0.77 min, respectively. It is clear that the addition of GPOE greatly enhanced the isothermal melt crystallization of PLA/GPOE blends.

The Avrami equation is frequently used to analyze the isothermal crystallization kinetics of polymers, according to which the relative degree of crystallinity X_t dependent crystallization time t can be expressed as [37,38],

$$X_t = 1 - \exp(-Kt^n) \quad (3)$$

where X_t is the relative degree of crystallinity, n is the Avrami exponent which depends on the nature of nucleation and growth geometry of crystallization, and K is the overall rate constant associated with both nucleation and growth contributions. The linear from Eq. (3) can be expressed as follows:

$$\log[-\ln(1-X_t)] = \log K + n\log t \quad (4)$$

The Avrami exponent n and the kinetic rate constant K can be obtained from the slopes and the intercepts, respectively.

In the case of the DSC experiment, X_t at t was defined as the ratio of the area under the exothermic curve between the onset crystallization time and t to the whole area under the exothermic curve from the onset crystallization time to the end crystallization time. Fig. 7(b) shows the Avrami plots of neat PLA and PLA/GPOE blends crystallized at 110 °C as an example, from which the Avrami parameters n and K could be obtained from the slopes and the intercepts, respectively. The obtained Avrami parameters of neat PLA and PLA/GPOE blends are summarized in Table 1 for comparison, from which it can be seen that the average values of n were around 2.33 for neat PLA and 2.77 for its blends at the investigated T_cs. The almost unaltered n values suggested that crystallization mechanism of PLA in the PLA/GPOE blends might not change. The values of K are also listed in Table 3.

Table 3. Crystallization kinetic parameters for pure PLA and PLA/GPOE blends based on the Avrami equation

PLA/GPOE (w/w)	T_c (°C)	n	K (min^{-n})	$t_{0.5}$ (min)
100/0	100	2.51	0.03	3.39
	105	2.19	0.05	3.32
	110	2.31	0.05	3.11
95/5	100	2.64	0.53	1.32
	105	2.88	0.68	1.01
	110	2.76	0.98	0.88
90/10	100	2.94	0.56	1.08
	105	2.56	0.72	0.98
	110	2.77	1.19	0.82
85/15	100	2.66	0.67	1.01
	105	2.71	0.77	0.96
	110	2.92	1.37	0.79
80/20	100	2.64	0.84	0.94
	105	2.85	0.85	0.93
	110	2.98	1.50	0.77

The crystallization half-time ($t_{0.5}$), the time required to achieve 50% of the final crystallinity of the samples, was introduced for comparing the overall crystallization rates. The value of $t_{0.5}$ was calculated by the following equation:

$$t_{0.5} = \left(\frac{\ln 2}{K}\right)^{1/n} \quad (5)$$

The crystallization rate can thus be easily described by the reciprocal of $t_{0.5}$. Fig. 8 panels a and b illustrate the variations of $t_{0.5}$ and $1/t_{0.5}$ with T_c for neat PLA and PLA/GPOE blends, respectively, from which the effects of T_c. As shown in Fig. 8, the values of $t_{0.5}$ decreased while the values of $1/t_{0.5}$ increased with increasing T_c for both neat PLA and its blends. Such variations indicate that the overall isothermal crystallization rate increased with increasing T_c. In addition, the values of $t_{0.5}$ for PLA/GPOE blends were lower than those of neat PLA at a given T_c, indicating again that the crystallization process of PLA/GPOE blends was accelerated after incorporation of GPOE, which should be due to the heterogeneous nucleation agent effect of in situ formed crystals [39]. The DSC results reported herein are consistent with the spherulitic morphology and growth studies in the following section. Note that the $1/t_{0.5}$ value increased with increasing GPOE content and exhibited the maximum value in the PLA/GPOE20 blend, suggesting that the GPOE loading had a significant effect of accelerating the crystallization of PLA/GPOE blends. Therefore, it was necessary to discuss the effect of the presence of GPOE and their loadings on the crystallization behavior of PLA/GPOE blends. The overall crystallization process of polymers generally involved both nucleation and growth. The crystals formed in the blends played two different or competing

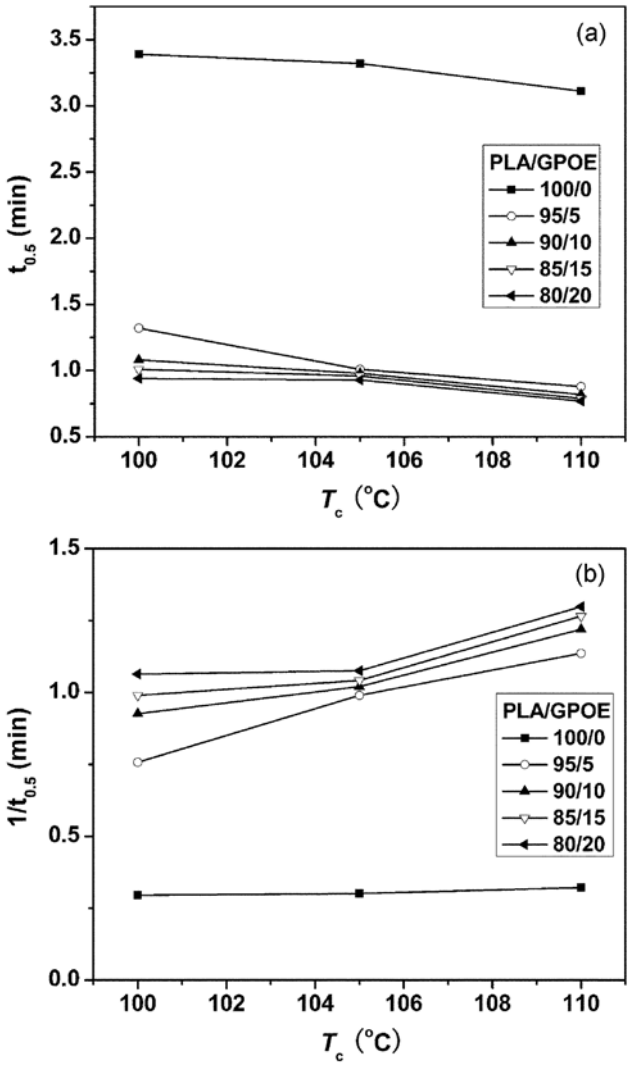

Fig. 8. Temperature dependences of (a) $t_{0.5}$ and (b) $1/t_{0.5}$ for neat PLA and various blends at various T_cs.

roles in affecting the crystallization process of PLA/GPOE blends. On the one hand, GPOE served as nucleating agent accelerate the isothermal crystallization of PLA/GPOE blends as discussed earlier. On the other hand, during crystallization process, the polymer chains had to overcome certain energy barriers to diffuse and attach onto the growing front of a crystal. The presence of GPOE might act as a physical cross-linking point to restrict the movement of chain segments and hinder the crystal growth process by imposing constraints on the surrounding polymer chains, especially when they have good interactions with polymer chains. The crystallization of PLA/GPOE blends was enhanced with increasing the GPOE loading because the nucleation effect induced by the GPOE predominated.

7. Crystalline Morphology

Spherulitic morphology of neat PLA and PLA/GPOE blends was studied with POM. Fig. 9 shows the spherulitic morphology of neat PLA and PLA/GPOE blends isothermally crystallized at 110 °C for 1 h. From Fig. 9(a), well-developed spherulites grow to about 50 μm in diameter, and the boundaries can be seen clearly for neat PLA

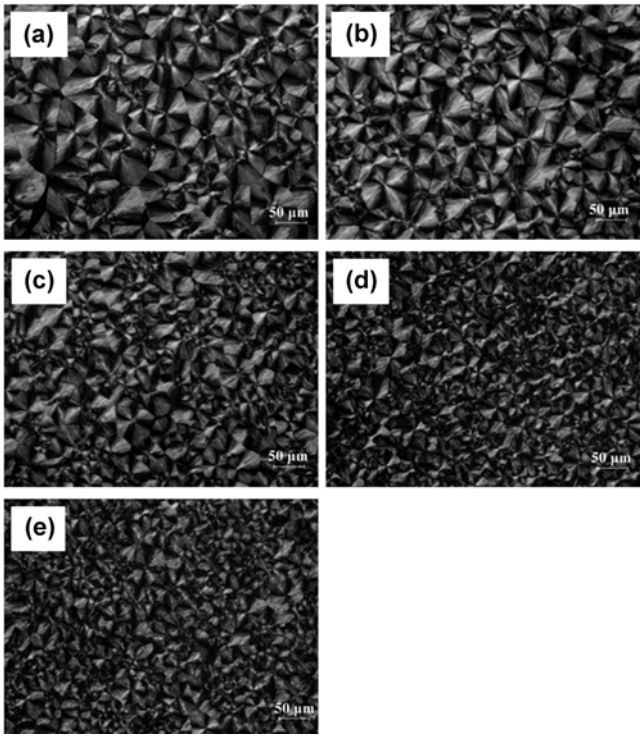

Fig. 9. Spherulitic growth process of neat PLA and PLA/GPOE blends at a crystallization temperature of 110 °C for 60 min: (a) 100/0; (b) 95/5; (c) 90/10; (d) 85/15; (e) 80/20.

sample. Fig. 9 panels (b), (c), (d), and (e) illustrate the POM images of the blends with the GPOE loading from 5 to 20 wt%. The presence of GPOE in PLA/GPOE blends resulted in the nucleating density of the spherulites being increased, the size of the spherulites decreased and obscurer spherulites boundaries. However, the content of GPOE in the blends did not show obvious effect on the morphology of spherulites. This result was in consistent with the crystallinity data from DSC (Table 2).

8. X-ray Analysis

Fig. 10(a) shows the WAXD patterns for the neat PLA and PLA/GPOE blends. It can be seen that the incorporation of GPOE does not modify the crystal structure of PLA in the blends relative to the neat PLA. The degree of crystallinity of PLA was calculated as follows [40,41].

$$W_{c,x}=\frac{\sum_i C_{i,hkl}(\theta)I_{i,hkl}(\theta)}{\sum_i C_{i,hkl}(\theta)I_{i,hkl}(\theta)+k_i C_a(\theta)I_a(\theta)}\times 100\% \quad (6)$$

where $W_{c,x}$ is the degree of crystallinity, $I_{i,hkl}(\theta)$ and $I_a(\theta)$ are the relative intensities of the crystalline and amorphous peaks, respectively, and $C_{i,hkl}(\theta)$ and $C_a(\theta)$ are the correction factors of the crystalline and amorphous peaks, respectively. On the basis of the X-ray diffraction intensity theory, K is the total correction factor, the calibration [$K=C_a(\theta)\times k_i$, where k_i is the relative scattering coefficient, which is a ratio of calculated diffraction intensity ($\sum I_{i,cal}$) to total scattering intensity ($\sum I_{i,total}$) for unit weight of crystalline polymer, and $k_i=\sum I_{i,cal}/\sum I_{i,total}$ ($k_i \le 1$)]. Here, $C_{i,hkl}(\theta)$ or $C_a(\theta)$ can be calculated by the following equation:

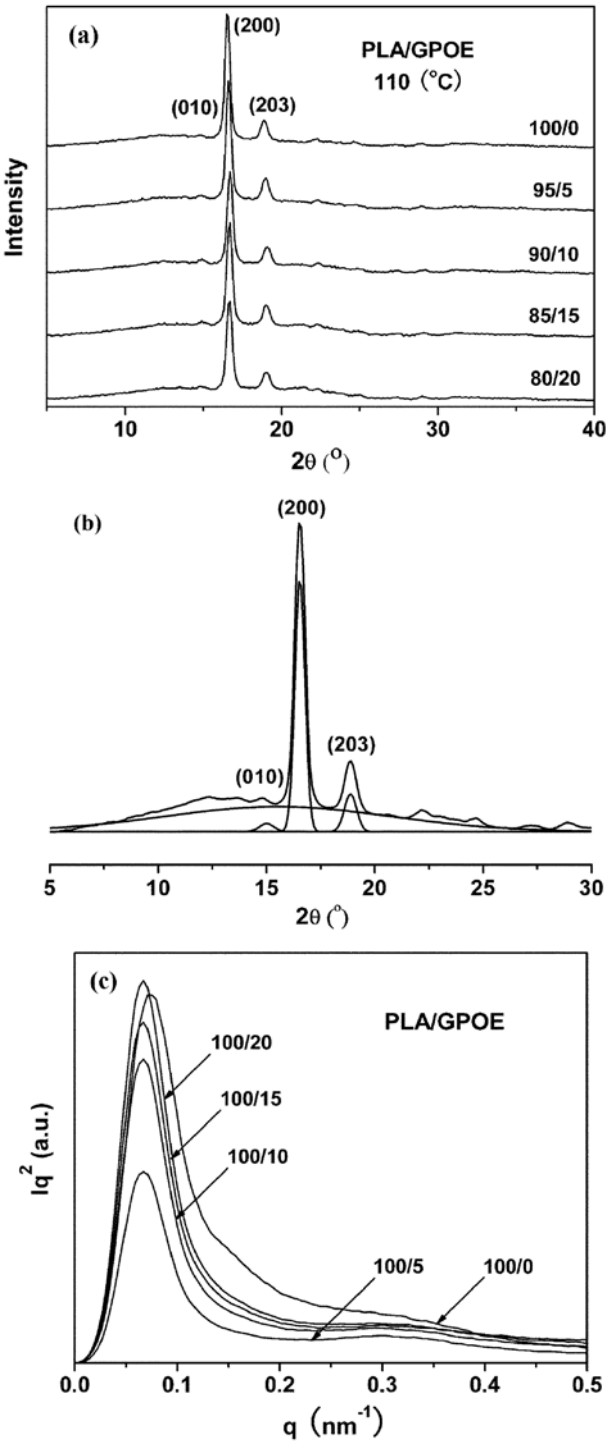

Fig. 10. Crystal X-ray analysis: (a) WAXD patterns of neat PLA and PLA/GPOE blends isothermally crystallized at 110 °C for 1 h, (b) magnification of the WAXD curve of PLA for the crystalline and amorphous portions, (c) Lorentz-corrected SAXS curves of neat PLA and PLA/GPOE blends.

$$C_{i,hkl}^{-1}(\theta) \text{ or } C_a^{-1}(\theta) = f^2 \cdot \frac{1+\cos^2 2\theta}{\sin^2\theta \cdot \cos\theta} \cdot e^{-2B(\sin\theta/\lambda)^2} = \sum_i N_i f_i^2 \cdot \frac{1+\cos^2 2\theta}{\sin^2\theta \cdot \cos\theta} \cdot e^{-2B(\sin\theta/\lambda)^2} \quad (7)$$

Table 4. X-ray diffraction data of pure PLA

hkl	A	010	200	203
2θ	15.6	15.0	16.5	18.9
$I_a(\theta)$ or $I_{i,hkl}(\theta)$	10000	200	4506	807
I	9000	181.9	5279	1356
T	0.93	0.93	0.92	0.89
$f^2=12f_H^2+12f_C^2+4f_O^2$	196.4	199.1	191.8	180.2
LP	106.1	114.4	93.73	71.4
$C(\theta)$	1	0.91	1.17	1.68
K	0.9			

Table 5. X-ray degree of crystallinity for the PLA/GPOE blends from isothermally crystallized at 110 °C for 1 h

PLA/GPOE	100/0	95/5	90/10	85/15	80/20
$W_{c,x}$ (%)	48.69	41.17	39.84	38.50	37.73

where f is the atomic scattering factor for one crystallographic structural repeating unit, f_i is the scattering factors of the ith atom, N_i is the number of ith atoms in a repeating unit, 2θ is the Bragg angle, the angle factor (LP)=$(1+\cos^2 2\theta)/\sin^2\theta\cos\theta$, the temperature factor (T)=$e^{-2B(\sin\theta/\lambda)^2}$, and 2B=10. f_i can be expressed approximately by

$$f_i(\sin\theta/\lambda) = \sum_{i=1}^{4} a_i \cdot e^{-b_i(\sin\theta/\lambda)^2} + C \quad (8)$$

where the values of a, b, and C are given in ref [42]

The total WAXD curve of neat PLA was resolved into crystalline and amorphous portions (Fig. 10(b)). From Eqs. (6)-(8), the X-ray diffraction data of the PLA/GPOE blends are shown in Table 4. $I_{hkl}=C_{i,hkl}(\theta)I_{i,hkl}(\theta)$ or $C_a(\theta)I_a(\theta)$ is the integrating intensity scattered over a suitable angular interval by the crystalline and the amorphous phases, respectively. The total atomic scattering factor was $f_{hkl}^2=3f_C^2+4f_H^2+2f_O^2$, where $k_i=0.9$, $C_a(\theta)=1$, and $K=k_iC_a(\theta)=0.9$. With the data of Table 4, Eq. (8) can be reduced to give Eq. (9).

$$W_{c,x} = \frac{0.91I_{010}+1.17I_{200}+1.68I_{203}}{0.91I_{010}+1.17I_{200}+1.68I_{203}+I_a} \quad (9)$$

where I_a is the intensity of amorphous peak.

The degree of crystallinity ($W_{c,x}$) for the neat PLA and PLA/GPOE blends was calculated with the Eq. (9), the values shown in the Table 5, which the crystallinity value in Table 2 exhibited $W_{c,x}>X_c$. The crystallinity determined from X-ray diffraction ($W_{c,x}$) was equal to the sum of the crystalline and interphase contents, while the measurement of fusion enthalpy by calorimetry (X_c) yields values which were equal to the crystalline content. Imperfections of crystals were not easily distinguished from the amorphous phase. Therefore, some disagreements among the quantitative results of crystallinity by different measurement methods were frequently encountered [43].

As shown in the WAXD pattern, after reactive compatibilization between PLA and GPOE, the reaction point worked as a physical cross-linking point, entangled structures in amorphous area impeded the transportation of macromolecular chains between polymer chains, restricting the crystalline ability of PLA and forming more

Table 6. Crystallite dimension of the neat PLA and its blends

PLA/GPOE (w/w)	ACS (Å)		
	(010)	(200)	(203)
100/0	124.8	170.8	143.6
95/5	121.5	167.7	142.6
90/10	121.1	166.3	141.3
85/15	120.8	165.3	139.7
80/20	120.4	163.1	139.3

amorphous phase, leading to the degree of crystallinity decreased.

The apparent crystal size (ACS) was estimated by Scherrer's equation [44]:

$$ACS = \frac{K\lambda}{\beta_{hkl}\cos\theta_{hkl}} \quad (10)$$

$$\beta = (B^2 - b^2)^{1/2} \quad (11)$$

where K, the Scherrer constant, takes a value of 0.9, λ is the wavelength of the X-ray (1.5418 Å) and θ is the Bragg angle. B is the half width in radians of the diffraction angle of the (010), (200) and (203), and b is the instrumental constant (0.1°). The calculated values of ACS are listed in Table 6. It is seen that the crystallite dimension of the blends was reduced relative to the neat PLA. This indicated that the presence of GPOE had strong influence on the crystallization of matrix PLA.

SAXS was used to investigate the crystal structure and macrostructure of neat PLA before and after blending with GPOE. Fig. 10(c) shows the Lorentz-corrected SAXS curves of the blends at various compositions annealed at 110 °C for 1 h. The long spacing d_{ac}, which was defined as the crystal layer thickness together with one interlamellar amorphous layer, measured along the lamella normal and calculated using Bragg Eq. (12) [45]. The crystal layer thickness d_c and the amorphous layer thickness d_a can be calculated using Eqs. (13) and (14), respectively.

$$d_{ac} = \frac{2\pi}{q_{max}} \quad (12)$$

$$d_c = d_{ac} \times X_{c,2} \quad (13)$$

$$d_a = d_{ac} - d_c \quad (14)$$

Here q_{max} represents the position of the intensity maximum in a SAXS pattern, $X_{c,2}$ represents the crystallinity of the samples of SAXS, which was derived from DSC measurement. The obtained q_{max}, d_{ac}, d_c and d_a values are summarized in Table 7. In Fig. 10(c), neat PLA exhibits a broader scattering peak, which can be observed around q=0.055 nm^{-1}. The scattering peaks gradually shifted in position to lower q values with increasing GPOE content, which indicated the d_{ac} values increased. In Table 7, the d_{ac}, d_c and d_a values were 114.6, 51.6, and 63.0 nm, respectively, for neat PLA. For the 80/20 PLA/GPOE blend, they became 123.7, 44.7, and 79.0 nm, respectively. It is obvious that all of the values of d_{ac} and d_a increased and the d_c values decreased with increasing GPOE content. However, the increase in d_a was large. For example, the increase in d_a was around 16.0 nm after blending 20 wt% GPOE as compared to that of neat PLA. Such significant increase in d_a suggested that amorphous GPOE might destroy the crystalline of PLA and reside in the interlamellar region of PLA spherulites.

Table 7. SAXS values of neat PLA and PLA/GPOE blends

PLA/GPOE (w/w)	q_{max} (nm^{-1})	X_c (%)	d_{ac} (nm)	d_c (nm)	d_a (nm)
100/0	0.055	45.04	114.6	51.6	63.0
95/5	0.050	39.84	123.7	49.3	74.4
90/10	0.050	38.72	123.7	47.9	75.8
85/15	0.050	38.02	123.7	47.0	76.7
80/20	0.050	36.14	123.7	44.7	79.0

CONCLUSIONS

PLA/GPOE blends were prepared successfully via simple melt compounding at various GPOE loadings. The elongation at break and impact strength were improved significantly compared with neat PLA. Scanning electron microscopy observation indicated that PLA could be significantly toughened by GPOE. The phenomenon of GPOE debonding from the PLA matrix, the cavitations and plastic deformation were able to explain the toughening mechanism perfectly. Isothermal melt crystallization kinetics of neat PLA and its various blends studied with DSC at various crystallization temperatures and analyzed by the Avrami equation. The overall crystallization rates were faster in the PLA/GPOE blends than that in neat PLA; however, the crystallization mechanism remained unchanged despite the presence of GPOE. The POM results showed that the number of PLA spherulites was higher in the PLA/GPOE blends than in the neat PLA; moreover, the size of PLA spherulites was smaller in the PLA/GPOE blends than that in the neat PLA. The increased nucleation density of PLA spherulites in the blends indicated that reaction point formed in situ could act as effective nucleation sites during the crystallization process of the PLA/GPOE blends. Furthermore, on the basis of the WAXD study, it could be concluded that the incorporation of GPOE did not modify the crystal structure of PLA in the blends relative to the neat PLA. The addition of GPOE decreased the degree of crystallinity of PLA. In addition, the crystallite dimension and crystal layer thickness of PLA decreased with the addition of GPOE. Consequently, GPOE could be an effective toughener for PLA.

ACKNOWLEDGEMENTS

This work was supported by the fund of Chinese Science Academy (Changchun Branch) (No. 2014SYHZ0019), Development and Reform commission of Jilin Province of China (No. 2015Y027), and the National Science Foundation of China (No. 51021003).

REFERENCES

1. L. Fambri, A. Pegoretti, R. Fenner, S. D. Incardona and C. Migliaresi, *Polymer*, **38**, 79 (1997).
2. K. J. Zhu, X. Z. Lin and S. L. Yang, *J. Appl. Polym. Sci.*, **39**, 1 (1990).
3. L. J. Han, C. Y. Han and L. S. Dong, *Polym. Int.*, **62**, 295 (2013).

4. R. Salehiyan and K. Hyun, *Korean J. Chem. Eng.*, **30**, 1013 (2013).
5. D. Cohn and A. H. Salomon, *Polymer*, **46**, 2068 (2005).
6. G. Theryo, F. Jing, L. M. Pitet and M. A. Hillmyer, *Macromolecules*, **43**, 7394 (2010).
7. L. V. Labrecque, R. A. Kumar, V. Dave, R. A. Gross and S. P. McCarthy, *J. Appl. Polym. Sci.*, **66**, 1507 (1997).
8. B. K. Chen, C. H. Shen, S. C. Chen and A. F. Chen, *Polymer*, **51**, 4667 (2010).
9. H. T. Oyama, *Polymer*, **50**, 747 (2009).
10. M. L. Robertson, K. H. Chang, W. M. Gramlich and M. A. Hillmyer, *Macromolecules*, **43**, 1807 (2010).
11. A. J. Nijenhuis, E. Colstee, D. W. Grijpma and A. J. Pennings, *Polymer*, **37**, 5849 (1996).
12. L. Jiang, M. P. Wolcott and J. W. Zhang, *Biomacromolecules*, **7**, 199 (2006).
13. Y. J. Li and H. Shimizu, *Macromol. Biosci.*, **7**, 921 (2007).
14. S. Ishida, R. Nagasaki, K. Chino, T. Dong and Y. Inoue, *J. Appl. Polym. Sci.*, **113**, 558 (2009).
15. M. E. Broz, D. L. Vanderhart and N. R. Washburn, *Biomaterials*, **24**, 4181 (2003).
16. M. Shibata, Y. Inoue and M. Miyoshi, *Polymer*, **47**, 3557 (2006).
17. M. Shibata, N. Teramoto and Y. Inoue, *Polymer*, **48**, 2768 (2007).
18. L. Jiang, M. P. Wolcott and J. Zhang, *Biomacromolecules*, **7**, 199 (2006).
19. A. Arostegui, M. Gaztelumendi and J. Nazabal, *Polymer*, **42**, 9565 (2001).
20. S. Zulfiqar, I. Fatima and M. I. Sarwar, *Korean J. Chem. Eng.*, **32**, 191 (2015).
21. G. H. Hu, Y. J. Sun and M. Lambla, *J. Appl. Polym. Sci.*, **61**, 1039 (1996).
22. Y. J. Sun, G. H. Hu, M. Lambla and H. K. Kotlar, *Polymer*, **37**, 4119 (1996).
23. H. Cartier and G. H. Hu, *J. Mater. Sci.*, **35**, 1985 (2000).
24. G. H. Hu, Y. J. Sun and M. Lambla, *Polym. Eng. Sci.*, **36**, 676 (1996).
25. E. W. Fischer, H. J. Sterzel and G. Wegner, *Colloid Polym. Sci.*, **251**, 980 (1973).
26. M. Zheng and X. Luo, *Polym. Plast. Technol.*, **52**, 1250 (2013).
27. H. L. Zhang, N. A. Liu, X. H. Ran, C. Y. Han, L. J. Han, Y. G. Zhuang and L. S. Dong, *J. Appl. Polym. Sci.*, ***125***, 550 (2012).
28. S. L. Sun, M. Y. Zhang, H. X. Zhang and X. M. Zhang, *J. Appl. Polym. Sci.*, **122**, 2992 (2011).
29. Y. P. Hao, H. Y. Liang, J. J. Bian, S. L. Sun, H. L. Zhang and L. S. Dong, *Polym. Int.*, **10**, 1002 (2013).
30. Y. L. Feng, Y. X. Hu, J. H. Yin, G. Y. Zhao and W. Jiang, *Polym. Eng. Sci.,* **53**, 389 (2013).
31. G. M. Van and J. Palmen, *Rheol. Bull.*, ***67***, 5 (1998).
32. D. F. Wu, Y. S. Zhang, M. Zhang and Y. Wei, *Biomacromolecules*, **10**, 417 (2009).
33. X. Wang, Y. Zhuang and L. Dong, *J. Appl. Polym. Sci.*, **126**, 1876 (2012).
34. V. L. Finkenstadt, C. K. Liu, P. H. Cooke, L. S. Liu and J. L. Willett, *J. Polym. Environ.*, **16**, 19 (2008).
35. A. Lazzeri and C. B. Bucknall, *J. Mater. Sci.*, **28**, 6799 (1993).
36. N. Dehghan, M. A. Tavanaie and P. Payvandy, *Korean J. Chem. Eng.*, **32**, 1928 (2015).
37. M. J. Avrami, *Chem. Phys.*, **8**, 212 (1940).
38. M. J. Avrami, *Chem. Phys.*, **9**, 177 (1941).
39. K. Anderson and M. Hillmyer, *Polymer*, **47**, 2030 (2006).
40. J. H. Yin and Z. S. Mo, *Modern Polymer Physics Science Press*, Beijing (2001).
41. Q. X. Zhang, Z. S. Mo, H. F. Zhang and S. Y. Liu, *Macromolecules*, **33**, 5999 (2000).
42. C. H. Macgillavry and G. D. Rieck, *International tables for X-ray crystallography*, Birmingham (1974).
43. H. L. Zhang, X. H. Sun, Q. Y. Chen, M. Q. Ren, Z. H. Zhang, H. F. Zhang and Z. S. Mo, *Chinese J. Polym. Sci.*, **6**, 589 (2007).
44. K.-S. Kim and M.-S. Kim, *Korean Chem. Eng. Res.*, **50**, 582 (2012).
45. H. Tsuji, K. Ikarashi and N. Fukuda, *Polym. Degrad. Stab.*, **84**, 515 (2004).